The Effects of Magnetic Treatment on the Tribological Behavior of AISI 1045 Steel under Lubricated Conditions

Xiang Xi, Yanqiu Xia & Yichao Hu

Accepted author version posted online: 19 Oct 2017.
Published online: 23 Jan 2018.

Submit your article to this journal

Article views: 110

View related articles

View Crossmark data

The Effects of Magnetic Treatment on the Tribological Behavior of AISI 1045 Steel under Lubricated Conditions

Xiang Xi, Yanqiu Xia, and Yichao Hu

School of Energy Power and Mechanical Engineering, North China Electric Power University, Beijing, P. R. China

ABSTRACT

The mechanical and tribological properties of pulse-magnetized and untreated AISI 1045 steel were studied comparatively. The microhardness and microstructures of treated and untreated steel samples were analyzed to evaluate magnetic treatment effects on the mechanical properties. Dislocation densities were calculated from X-ray diffraction data according to the Williamson-Hall method. Tribological tests were conducted using a ball-on-disk reciprocating friction and wear tester. Scanning electron and energy-dispersive microscopies were used to analyze the morphologies and elements of worn surfaces. Dislocation densities of AISI 1045 steel were found to increase by 16.5% after magnetic treatment. Treated steel performed better under polyalphaolefin (PAO) base oil lubrication with each of five additives, especially when oleic acid was 0.2 and 1.5% (by mass), and the wear scar width and friction coefficient of treated samples were 46.9 and 16.4% lower than those of the untreated samples, respectively. Morphological analyses indicated that micromagnetic fields generated during friction tests not only promoted oxidation of the worn surface and debris but also produced thinner tribofilms that included chemical and adsorbed films.

Introduction

In modern society, metal life is a precondition for mechanical parts to work well over time. In particular, AISI 1045 steels are widely used for the production of almost all mechanical parts, such as gears, rods, and bolts, because of its good machining performance and its processing and economic characteristics (Haftlang, et al. *(1)*). However, such parts are frequently subjected to wear because of their low surface hardness and poor wear resistance. Previously, our research group has focused on AISI 1045 steels and found some surface modification methods that improve antiwear properties. For example, nickel coatings electrodeposited on AISI 1045 steel substrates exhibit excellent tribological properties that are attributed to their high hardness (Xia, et al. *(2)*). Xia, et al. *(3)*, *(4)* have revealed that AISI 1045 steel shows better wear resistance after being copermeated with lanthanum and boron with the aid of a solid permeation technique and that laser heat treatment can also be used to increase the hardness of AISI 1045 steel. In addition, diamond-like carbon coatings have attracted attention for their effective enhancement of AISI 1045 steel surfaces by increasing its hardness and improving wear resistance (Jia, et al. *(5)*–*(7)*). However, these methods have unresolved disadvantages, such as high costs and long treatment times. We are focusing on pulsed magnetic treatment that exhibits advantages such as being pollution free and having high effectiveness. Fortunately, many studies have verified that proper magnetic treatment increases steel hardness and, consequently, enhances wear resistance as

well. Magnetic treatment has been successfully applied to improve cutting tool strength by magnetizing before or during the cutting process (Ma, et al. *(8)*, *(9)*; Liang, et al. *(10)*). AISI 1045 steel is a kind of ferromagnetic material that can be magnetized when exposed to an external magnetic field and then remain a permanent magnet because the imposed magnetization is preserved after magnetic field removal. Some studies have focused on magnetic treatment effects on materials' mechanical performance (Nabi, et al. *(11)*; Mikhalitsyna, et al. *(12)*). A series of high-speed steel tests by Ma, et al. *(9)* revealed that the subjected force of dislocations generated by magnetic treatment overcomes the centripetal restoring force and Peierls stress of dislocations. Increases in dislocation density caused by dislocation multiplication and dislocation slip would help to improve a material's microhardness. Cai and Huang *(13)* have shown that a magnetic field creates conditions for dislocation depinning that drives dislocations moving further and faster, resulting in residual stress reduction. Liang, et al. *(14)* have proposed that, after pulsed magnetic treatment, the lattice of M42 high-speed steel material is distorted, carbides are precipitated, and the microstructure and crystalline grains are refined, resulting in increased Rockwell hardness and microhardness. Other researchers have studied the tribological properties of steels in dry friction experiments, the results of which have shown that a magnetic field could improve tribological properties. The main mechanisms for these effects are summarized as follows. The main effect of a magnetic field is to increase the

---

Color versions of one or more of the figures in the article can be found online at www.tandfonline.com/utrb.
Review led by K. Fukuda.

oxygen density and accelerate oxidation on worn surfaces, which can then further decrease both the abrasion ratio and friction coefficient (Wei, et al. (15); Tharajak and Nicomrat (16); Babutskyi, et al. (17)). In addition, a magnetic field enhances oxygen activity and finely oxidized particles are attached to worn surfaces, thus preventing overwear (Han, et al. (18); Jiang, et al. (19)). The study of metal surfaces in micromagnetic fields associated with the tribological phenomenon is of considerable scientific and practical interest. However, most previous reports have been conducted in the presence of an external magnetic field, and there is little literature analyzing the relationship between tribological processes on magnetized material surfaces. Furthermore, in practice, most mechanical parts work under lubricated conditions, and there remains a lack of knowledge regarding wear mechanisms involving lubricated magnetic-treated steel. In this study, material property tests were carried out to investigate these mechanisms as well as the tribological performance of nonmagnetized and magnetized specimens during lubricated wear tests.

In this study, magnetized and nonmagnetized samples were compared in wear and tribological tests while under lubrication with polyalphaolefin (PAO) base oil with the addition one of the following five additives: molybdenum dithiocarbamate (MoDTC) and zinc dialkyl dithiophosphate (ZDDP), the most widely researched additives for good wear resistance (Du, et al. (20); Wang, et al. (21); Parsaeian, et al. (22)); oleic acid, usually used as a lubricant additive because of its alcohol and carboxylic functional groups, which can generate an adsorption film on the metal surface to improve tribological properties (Miyake, et al. (23)); ashless organic phosphonate (AOP), an extreme-pressure antiwear additive, which is widely added to industrial gear oil; and leaf-surface wax, which is prevalent in plants and considered a new kind of biodegradable additive (Xu, et al. (24)). Most common oil materials might be hard to degrade or degradation resistant in the environment. Moreover, many additives containing the elements P, S, or halogen are not only degradation resistant but are noxious to nature and living creatures, although they are effective in lubrication. It is increasingly significant to discover environmentally friendly lubricating materials to reduce these disadvantages. Therefore, our research group focuses on leaf-surface wax as an environmentally friendly additive. Xia, et al. (25) have revealed that excellent tribological properties afforded by leaf-surface waxes are mainly due to its organic composition, which includes fatty acids, alcohols, ketones, and esters. In this study, extracted Korean pine (KP) leaf-surface wax was chosen as a source for this additive.

Experimental details

Magnetic treatment equipment

The work principle of the pulsed magnetic treatment equipment is shown in Fig. 1. The device consisted of two sections, including a pulsed-power system and a magnetic field generator. The magnetic generator had a double-choke H structure and included a movable core, a fixed core, coils, and an adjustable knob. Specimens were placed in the air gap between the movable and fixed cores, and the gap distance was regulated using the adjustment knob. The pulsed-power generator
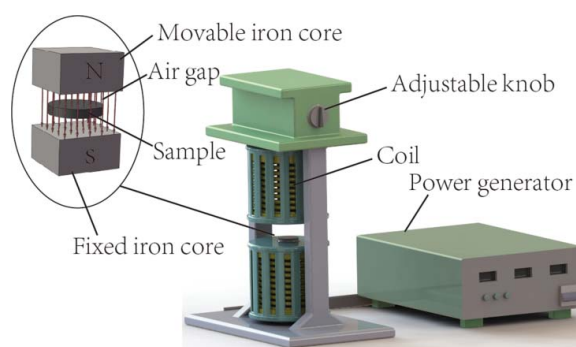

Figure 1. Pulse magnetic treatment equipment.

provided two current waveforms, a sine and a unidirectional square form, but only the latter was used here. The parameters of a magnetic treatment are shown in Table 1 according to preliminary research.

Experiments

AISI 1045 steel samples used had a diameter and height of 24 and 7.8 mm, respectively. The organization and performance of tests on samples before and after magnetic treatment followed the procedures described below. First, the samples were sanded with abrasive paper (grit 2,000) to remove surface rust and then polished using diamond lapping paste (1.5 μm) to a final roughness, R_a, of 0.05 μm. Then, samples were cleaned with petroleum ether. Next, a 4% nitric acid alcohol solution (by volume) was used to reveal the sample microstructure. Finally, the fine texture and microstructure of samples were observed by optical microscopy.

The base oil lubricant was synthetic oil polyalphaolefin (PAO40) of viscosity 387.4 mm^2/s at 40°C and 40.5 mm^2/s at 100°C. The addition of each additive was as follows. The MoDTC was added into the oil at 1% (by mass). The antiwear additive was ZDDP, containing Zn, P, and S at 10.0, 8.0, and 16.0% by mass, respectively. Oleic acid was added to the PAO40 lubricant. AOP was added to the base oil. KP plant samples were collected in Beijing, China. Before distilling the leaf-surface wax, the leaves were cleaned, dried, and then dipped in chloroform for 8–15 s at ambient temperature. The extract was then filtered, dried, and concentrated to yield wax (a solid powder). Finally, KP wax samples were added to the oil. Gas chromatography–mass spectrometry was adopted to analyze the primary component of the KP wax. After comparison between the strongest peak, which was determined as the metric, and the remaining peaks, the content of each peak could be inferred. The content of KP wax is provided in Table 2.

Table 1. Parameters of magnetic treatment.

Parameters	Value
Magnetic field intensity (Gs)	320
Margination time (s)	30
Output voltage (V)	380
Output current (A)	20
Frequency (Hz)	50

Table 2. Composition of the KP wax.

Constituents	KP wax (%)
Olefins	2
Alkanes	16
Esters	1
Alcohols	62
Acids	4

It can be seen that the most abundant components are alkanes and alcohols, whereas the acid and ester contents are low.

Microhardness experiments were carried out using a micro-hardness tester with a load of 0.98 N and load application time of 10 s.

In using the Williamson-Hall method, dislocation densities before and after magnetic treatment were obtained by analyzing X-ray diffraction peak profiles (Williamson and Smallman (26)). There was a close relationship between X-ray and the microstructure of material, including dislocation density and grain size and distribution. For example, the material texture is related to the relative height of diffraction lines and the material grain size and dislocation density reflect diffraction line widths (Hahn, et al. (27)). The Williamson-Hall method is a straightforward means of obtaining a material's microdistortion and grain size by separating the length and strain–stress effects of several diffractions, and it is adequate to analyze the influence of magnetic treatment on dislocation densities. X-ray diffraction experiments were carried out on electropolished sections of treated and untreated specimens utilizing an X-ray diffractometer under the conditions of Cu Kα radiation, 30 kV, 20 mA, and scan rate of 10°/min. The horizontal axis values are the angles between incoming light and reflected light; the vertical axis values are the number of particles received by the detector. The grain sizes of treated and untreated samples were calculated according to the Scherrer equation. These calculations of X-ray diffraction (XRD) analysis are shown in Table 3.

In the above method, the diffraction peak broadening $\delta_{e,hkl}$, which is caused by the variations in interplanar distances, is characterized by the average microstrain:

$$\delta_{e,hkl} = 2e \tan\theta_{hkl} \quad [1]$$

where e is the microstrain and θhkl is the diffraction peak's Bragg angle. Diffraction peak broadening, which is caused by the grain size in the coherent region, is calculated by the

following equation:

$$\delta_{D,hkl} = \frac{\lambda}{D\cos\theta_{hkl}} \quad [2]$$

where λ is the radiation wavelength and D is the apparent size parameter. It is assumed that there is a linear relationship between particle size and microstrain contributions with an observed line breadth (Biju, et al. (28)):

$$\delta_{hkl} = \delta_{D,hkl} + \delta_{e,hkl} \quad [3]$$

with δ_{hkl} the wide quantization of diffraction peak (hkl) that can be obtained by the following equation:

$$\delta_{hkl} = \sqrt{\left(\delta_{hkl}\right)^2_{measured} - \delta^2_{instrumental}} \quad [4]$$

where $(\delta_{hkl})_{measured}$ is the test sample's full-width half-maximum (FWHM), and $(\delta_{hkl})_{instrumental}$ is the FWHM of a standard iron sample (fully annealed pure iron). Finally, the Williamson-Hall equation gives

$$\delta_{hkl} \frac{\cos\theta_{hkl}}{\lambda} = \frac{1}{D} + 2e\frac{\sin\theta_{hkl}}{\lambda} \quad [5]$$
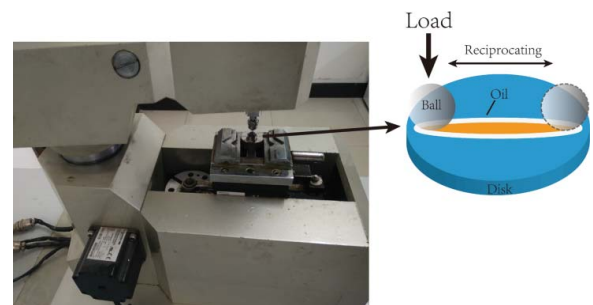
According to Eq. [5], the microstrain e was obtained from the slope of the line drawn by using straight line fitting to plot the value of $\delta_{hkl}\frac{\cos\theta_{hkl}}{\lambda}$ as a fraction of $2\frac{\sin\theta_{hkl}}{\lambda}$. Then, dislocation densities were calculated using the following equation (Tan, et al. (29)):

$$\rho = 14.4\frac{e^2}{b^2} \quad [6]$$

where ρ is the dislocation density and b is the Burger vector (for ferrite, b is 0.248 nm).

Tribological tests

The tribological properties of magnetic-treated specimens were probed quantitatively by conducting a range of tribological tests under lubrication conditions using a ball-on-disk reciprocating friction and wear tester (Fig. 2). The concentrations of additives by weight fraction in the oil were varied from 0.2 to 3% to investigate the influence of concentration on friction and wear.

Table 3. Calculations of XRD analysis.

Samples	Planes	2θ (°)	FWHM (°)	D (nm)
Untreated	(110)	44.980	0.252	33.74
	(200)	65.183	0.354	26.34
	(211)	82.503	0.426	24.53
Treated	(110)	44.981	0.274	31.03
	(200)	65.160	0.437	21.33
	(211)	82.542	0.449	22.74

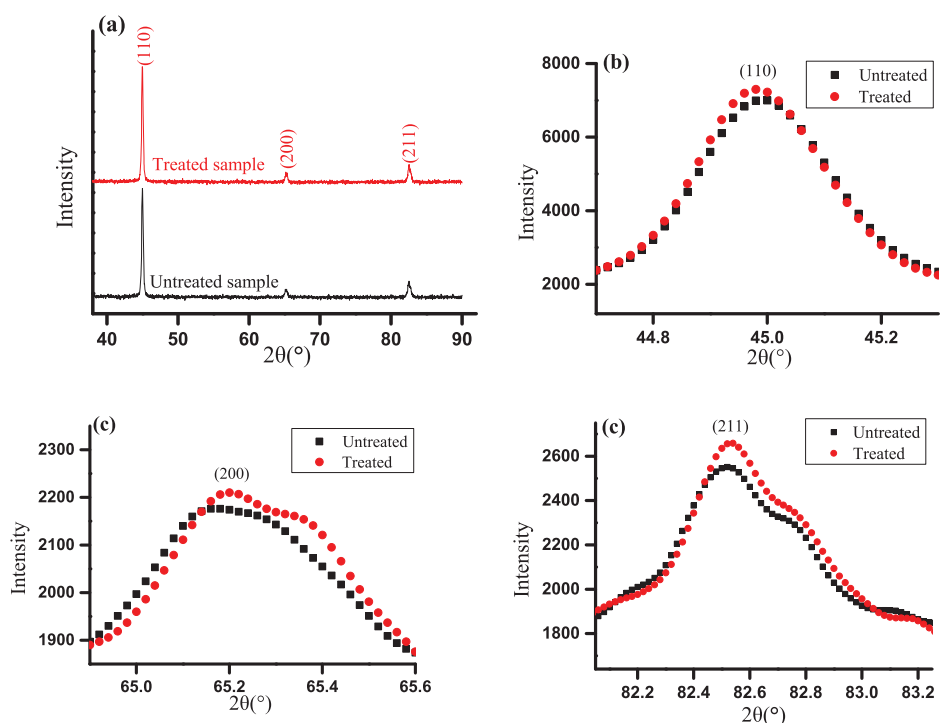**Figure 2.** MFT-R4000 reciprocating friction and wear tester.

Figure 3. X-ray diffraction patterns and diffraction peak profiles of untreated and treated samples. (a) X-ray diffraction patterns, (b) (110) diffraction peak, (c) (200) diffraction peak, (d) (211) diffraction peak.

The capacity of load-carrying tests was performed with normal loads of 50, 100, 150, and 200 N under oil lubrication with the best concentration of each additive. A frequency of 5 Hz was selected with a test duration of 30 min. Before and after every tribological test, all samples and balls were cleaned in petroleum ether for 15 min in an ultrasonic cleaner. A controlled amount of lubricant—that is, several oil drops—was then spread on a disk sample before each tribological test. The friction coefficient was recorded automatically by a computer attached to the friction and wear tester. An optical microscope was used to obtain disk wear scar widths. Triplicate tests were performed and wear scar average values are included in the results. Disk surface topography and elements present in scratches were analyzed using a scanning electron microscope and an energy-dispersive spectrometer (Vickers hardness [HV]: 10 KV).

The balls were made from AISI 52100 steel, with identical mechanical, thermal, and surface characteristics. These standard steel ball bearings were 5 mm in a diameter, with an HV of 710 and a surface roughness, R_a, greater than 0.03 μm.

Experimental results

Effects of magnetic treatment on microhardness and dislocation density

Microhardness tests revealed that sample microhardness showed some improvement after magnetic treatment. The average microhardness values of untreated and treated samples were determined to be 204 and 220 HV, respectively, which meant that treated samples would have better wear resistance than untreated samples. Some studies have pointed out that increases in microhardness after magnetic treatment could be

ascribed to high dislocation densities generated by the powerful magnetic field driving force (Ma, et al. (9)).

X-ray diffraction patterns and three diffraction peak profiles ((110), (200), and (211)) of untreated and treated samples are shown in Fig. 3. These three peak profiles were extracted from X-ray diffraction patterns to study the changes in microstrain in untreated and treated samples. Compared to untreated samples, the three peak profiles of treated samples broadened, which was attributed to increased steel microstrain. The observed deviation in the (200) and (211) peak positions was considered to indicate differences in samples' inner residual stresses (Wang and Wang (30)).

Dislocation densities of untreated and treated samples were calculated according to the Williamson-Hall method using
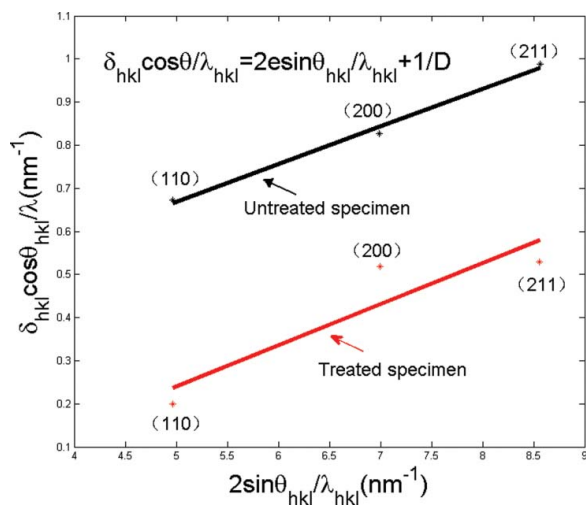

**Figure 4.** Consequence of linear fitting.

Table 4. Dislocation densities of untreated and treated samples.

Item	Untreated	Treated
Dislocation density (10^{12} m^{-2})	1.776	2.126

Eq. [6] and with the linear fitting results shown in Fig. 4. Based on the figure, slopes of the two lines were calculated as 8.71 and 9.53; the dislocation densities of untreated and treated samples were calculated and are shown in Table 4. There was an obvious increase in dislocation density of ~16.5% after magnetic treatment. Under magnetic force effects, new lattice defects emerged due to the balanced destruction of the lattices. Considered in terms of energy, magnetic fields can increase the flexibility of dislocation movement, which will accelerate the process of residual stress release in materials (Klamecki (31)). From these effects, lattices constantly reproduce, slide, and climb and, consequently, the dislocation density increases.

Influences of microstructure

The abrasion-resistant mechanism was revealed by analyzing the microstructures of untreated and treated samples (Fig. 5). AISI 1045 steel is hypoeutectoid steel that contains ferrite and pearlite structures. Compared to Fig. 5a, Fig. 5b indicates that the ferrite became finer and these finer grains were observed in
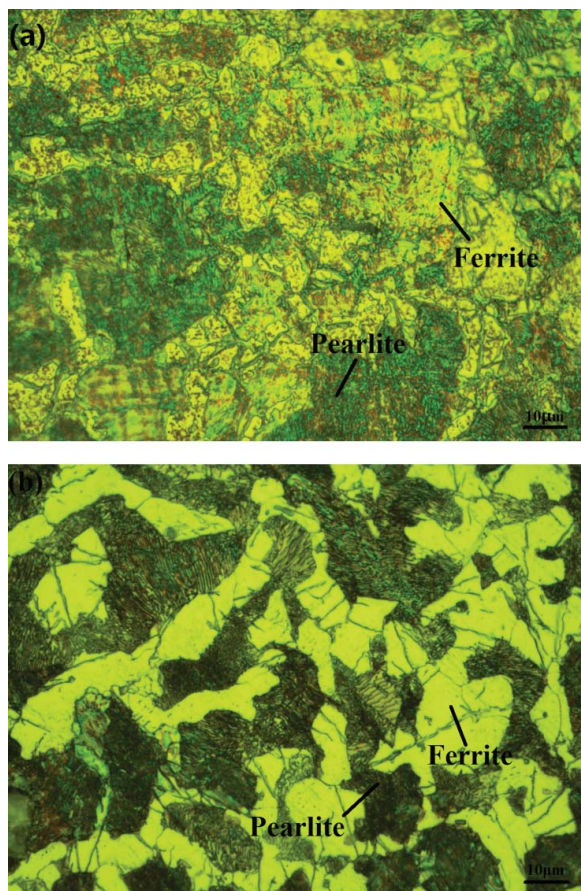

Figure 5. Microstructure of the AISI 1045 steel sample (a) before and (b) after magnetic treatment.

a network-like distribution along the grain boundary of the original austenite after magnetic treatment. According to the calculations of XRD analysis, the average grain sizes of treated samples are lower than those of untreated samples. Thus, it was inferred that magnetic treatment refined the ferrite crystals. Viewed from the nucleation driving force point, magnetic field effects on refined grains are due to interactions between the magnetic field and iron atoms' spin magnetic moment (Ma, et al. (32)). In other words, magnetic field effects result in an increase in mean nucleation, which might have been an effective means for refining ferrite grains. In general, hardness increased and antiwear properties improved with ferrite grain refinement.

The energy-dispersive spectroscopy (EDS) analysis results of untreated and treated samples are shown in Fig. 6. It can be found that the O concentration of the treated sample is higher than that of the untreated sample, indicating that magnetic treatment can increase oxidation on the sample's surface.

Influences of concentration

The coefficient and wear scar width are known affected by the concentration of additives. Figure 7 shows the friction coefficient and wear scar width of untreated and treated disks under PAO40 lubrication at varying concentrations. In both untreated and treated disks, the tendency of friction coefficients under all additive-modified lubricants was the same, such that friction coefficients initially decreased and then increased as the concentration increased. As a result, clear friction reduction effects were obtained when concentrations were optimal. In particular, when the oleic acid concentration was 1.5%, the magnetic-
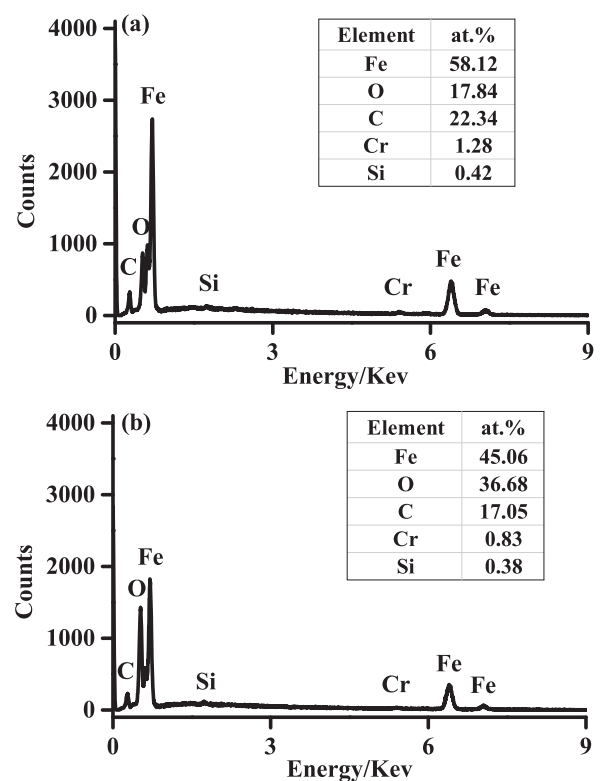
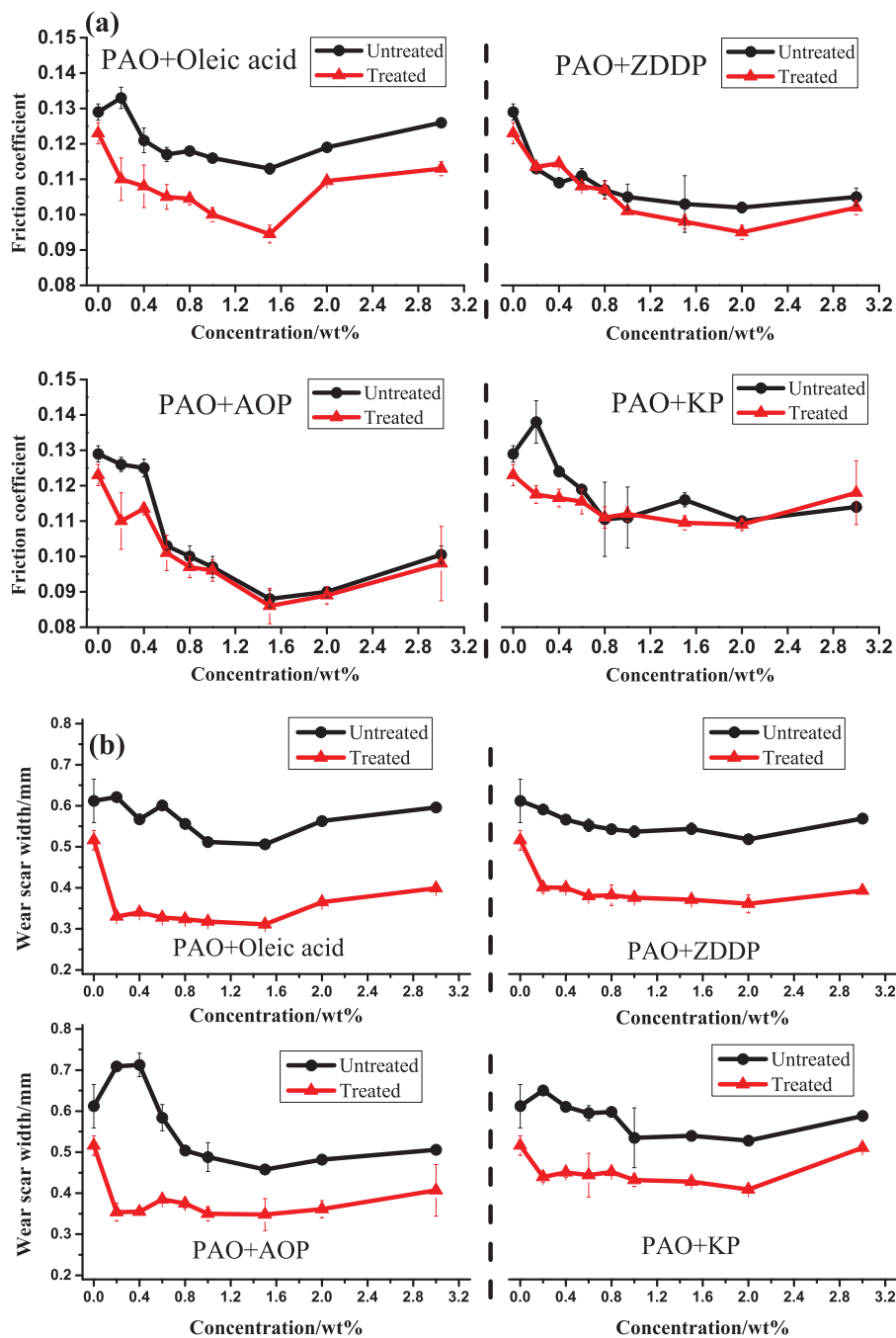**Figure 6.** EDS spectra of unworn (a) treated and (b) untreated samples.

Figure 7. Variation in the (a) friction coefficient and (b) wear scar width as function of additive concentration at ambient temperature and humidity (load = 50 N; frequency = 5 Hz; stroke = 5 mm; duration = 30 min).

treated samples exhibited improved antifriction properties, which were ~16.4% lower than that of untreated samples. For both untreated and treated disks, the neat PAO40 base oils exhibited high erosion rates. For all concentrations, the wear scar widths of treated disks were significantly lower than those of untreated disks. Among all results, the AOP-modified lubricants exhibited the greatest wear-reducing results, by ~32.6% as the concentration increased from 0 to 1.5%. It was also found that wear scar widths of untreated and treated disks were similar as the concentrations of ZDDP, AOP, or KP increased from 0 to 3%.

Influences of normal load

Figure 8 presents average friction coefficients and wear scar widths of untreated and treated samples under oil lubrication with 1.5% oleic acid, 2% ZDDP, 1% MoDTC, 1.5% AOP, or 2% KP, at multiple normal loads and ambient temperature. The mean friction coefficients of treated disks were lower than those of untreated disks under all additive-modified lubricants. It was also found that, regardless of normal load, additives in the base oil produced considerable friction coefficient reductions for treated disks in comparison to the base oil. Wear scar widths of treated disks were still relatively smaller than those of untreated
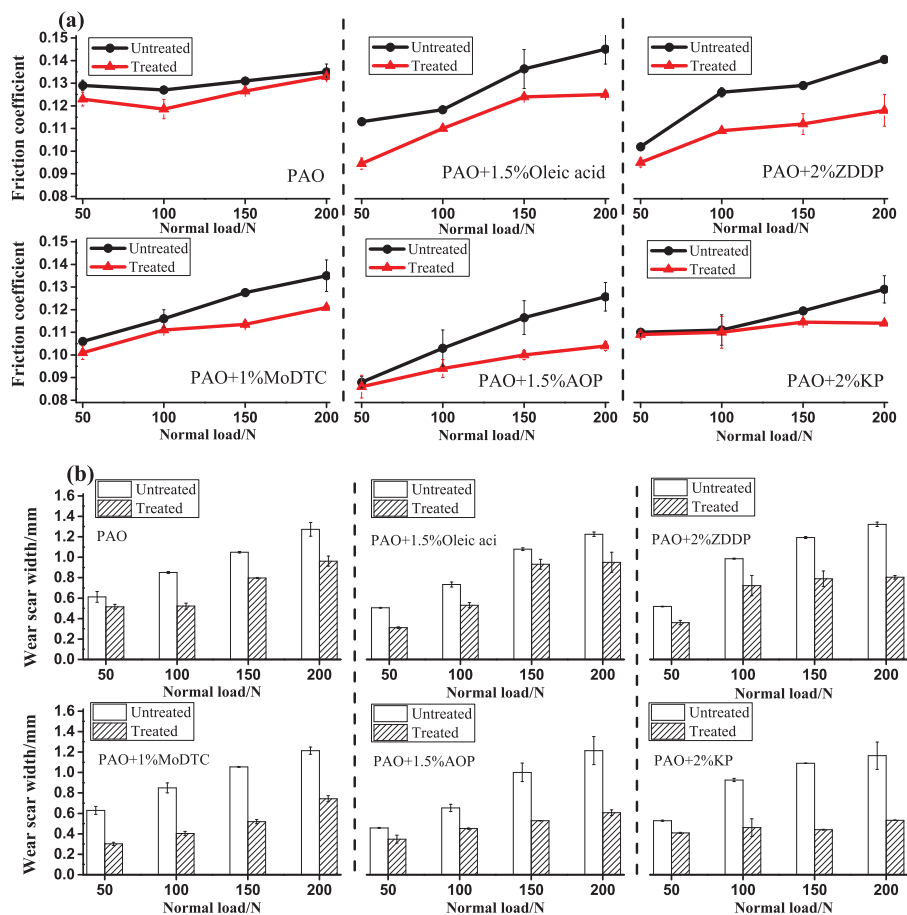
Figure 8. Effect of normal load on average (a) friction coefficient and (b) wear scar width under lubrication with the base lubricant and the base lubricant containing additives (frequency = 5 Hz; stroke = 5 mm; duration = 30 min).

disks, indicating better wear resistance among treated disks. In particular, under 2% KP lubrication, wear scar widths of treated disks were ~54.3% lower than those of untreated disks when the normal load was increased to 200 N. The outstanding antiwear property of treated disks has been commonly interpreted as the function of a magnetostriction effect, which leads to changes in microscopic structures, such as grain refinement, which is more uniform after magnetic treatment.

Wear surface microanalysis

Understanding of the wear mechanism on untreated and treated disk surfaces lubricated with additive-modified lubricants was explored by conducting scanning electron microscopy (SEM) and EDS analyses, respectively, of the worn surfaces. Figure 9 compares SEM images of the worn surfaces of untreated and treated disks generated under reciprocating sliding conditions. A large number of deep ploughing grooves and large pits were found scattered on worn surfaces of untreated disks, implying that these surfaces were badly damaged. This phenomenon was considered to function such that, with increased normal load, the tribological film easily cracked and flaked off in the form of blocks from the disintegrating material and formed deep pits on the worn surfaces. In addition, hard debris scattered on the worn surfaces acted as abrasive grains, resulting in deep surface

grooves. In contrast, only some shallow grooves and small pits were found on the worn surfaces of treated disks lubricated with all additive-modified lubricants. The factors explaining why treated disks showed better antiwear properties are shown in Fig. 10. On the one hand, the oxygen content of treated disks was higher than that of untreated disks, which indicated that oxide layers were more easily formed on the worn surfaces of material after magnetic treatment and, consequently, restrained material grooving and pitting (Stolarski and Makida (33)). On the other hand, tribochemical reactions, including the generation of a tribofilm containing typical elements such as S, Mo, N, and P, might have more easily occurred on the worn surfaces of treated disks (Kano, et al. (34); Okubo, et al. (35); Wang, et al. (36); Feng and Xia (37); Yang, et al. (38)). This tribofilm appeared to improve friction-reducing and antiwear properties. Based on the above results, it was concluded that abrasive and adhesive wear were the dominant wear mechanisms for untreated and treated disks lubricated by all additive-modified lubricants.

Discussion

The above experimental results determined that magnetic treatment effectively improved the mechanical and tribological properties of AISI 1045 steel materials, including increases in microhardness and dislocation density, which resulted in
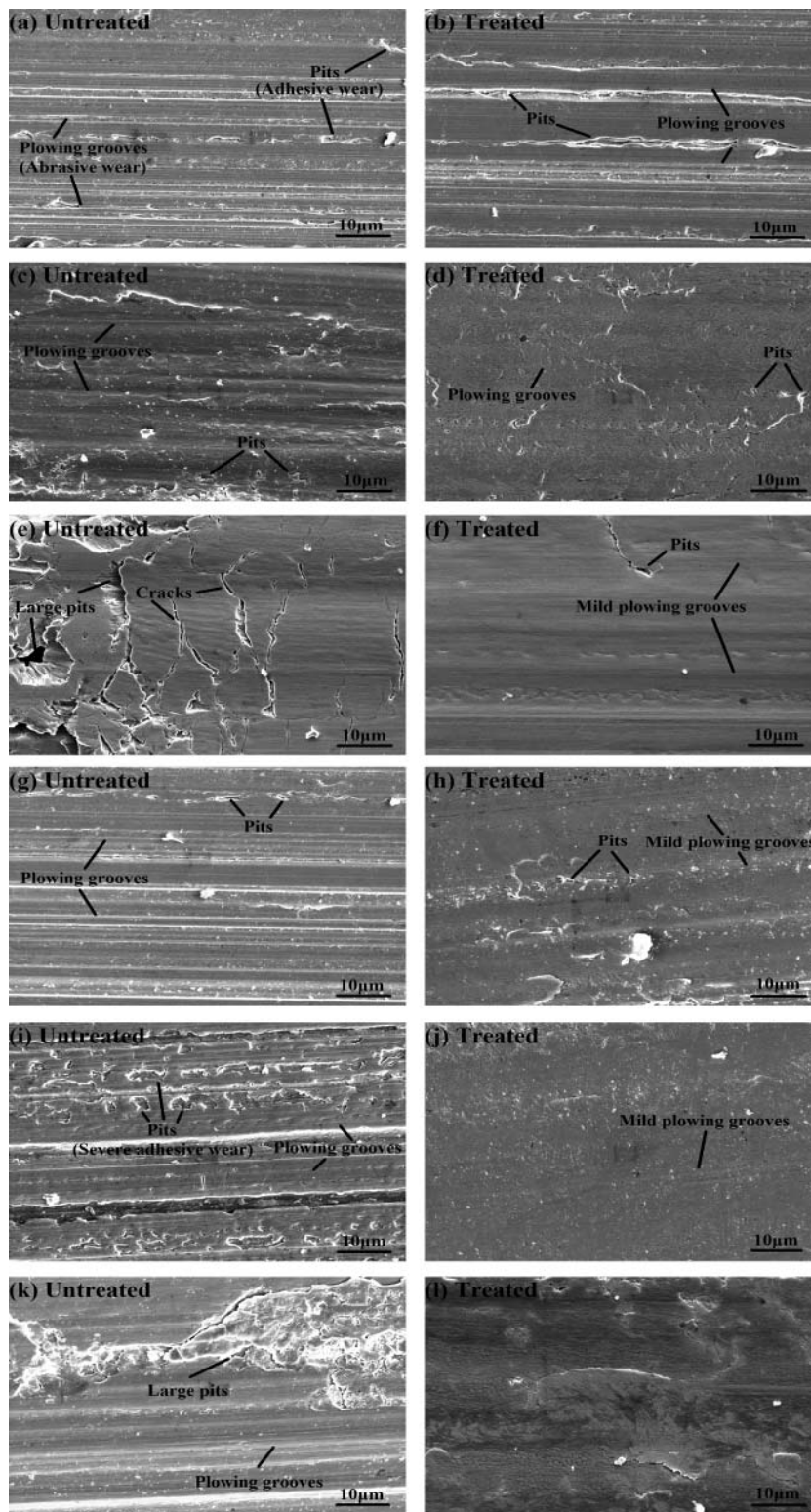
Figure 9. SEM morphologies of the worn surfaces of disks lubricated with (a), (b) PAO; (c), (d) PAO + 1.5% oleic acid; (e), (f) PAO + 2% ZDDP; (g), (h) PAO + 1% MoDTC; (i), (j) PAO + 1.5% AOP; and (k), (l) PAO + 2% KP.

generating better friction-reducing and antiwear properties. The property-changing mechanism, the relationships between the treatment effect and friction chemical reactions, and the static and dynamic mechanisms are clarified in the discussion below.

Static mechanism

A model of the magnetostrictive mechanism is shown in Fig. 11. The magnetostrictive effect in ferromagnetic materials is generated by a balance between material elastic energy and
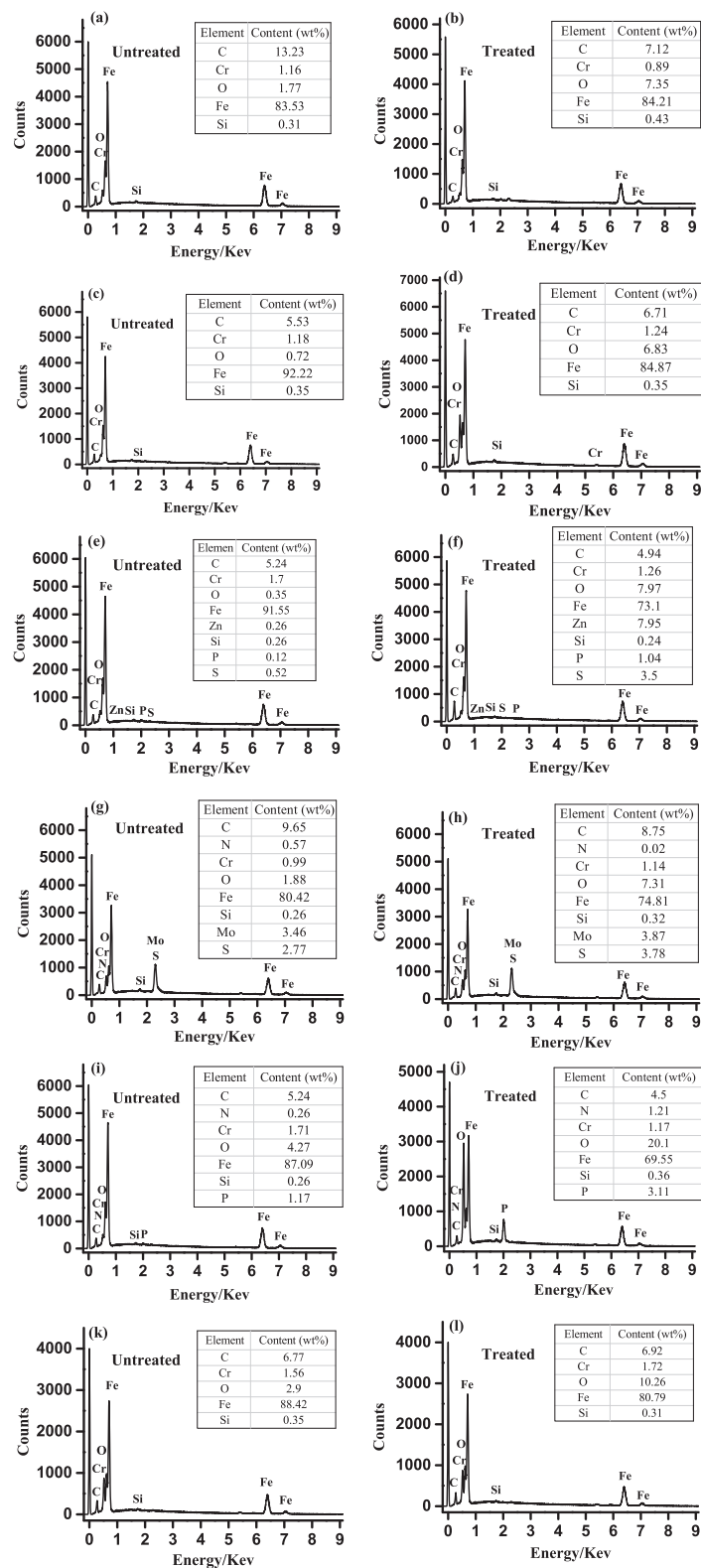
Figure 10. EDS quantification of the worn surfaces of disks lubricated with (a), (b) PAO; (c), (d) PAO + 1.5% oleic acid; (e), (f) PAO + 2% ZDDP; (g), (h) PAO + 1% MoDTC; (i), (j) PAO + 1.5% AOP; and (k), (l) PAO + 2% KP.

spin and orbital coupling energies. Without the effects of an external magnetic field, atoms align at random angles to one another. When an external magnetic field is applied along a sample's vertical axis, the magnetic moments of the electron clouds line up with the direction of the external magnetic field after deflections. According to a previous report (Filho, et al.

(39)), under magnetic field effects, the magnetostrictive effect on ferrite crystals is linked not only to magnetization but also to crystal orientation. The report also revealed that different crystal orientations might have different influences on the magnetostrictive effect, which leads to lattice distortion of ferrite and austenite as well as the generation of elastic distortional
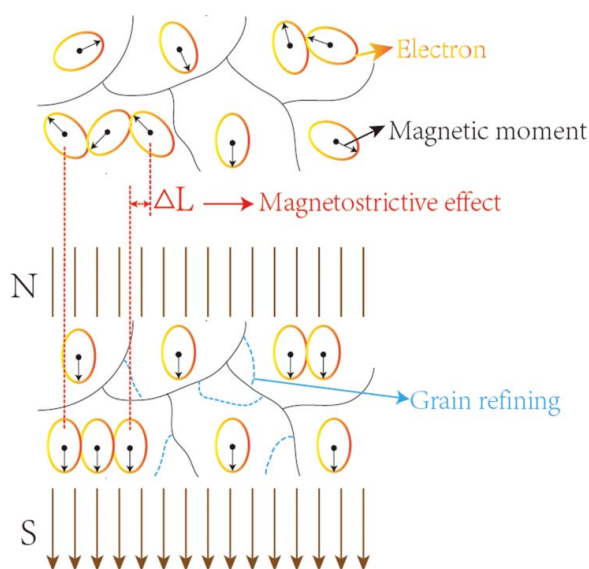
Figure 11. Schematic illustration of the magnetostrictive effect.

energy. This energy improves ferrite transformation and increases the ferrite nucleation rate, which can refines ferrite grains (Ma, et al. (32)). All of these microstructural changes lead to increased dislocation density, which increases material microhardness and improves wear resistance properties.

Dynamic mechanism

Figure 12 shows a schematic of dynamic friction and the wear mechanism as well as additive dispersal in oil; oxidation plays a key role in decreasing friction and wear. In this experiment, friction debris on magnetized disks contained more oxygen according to EDS analysis, which was similar to results reported in other studies (Wei, et al. (15); Tharajak and Nicomrat (16); Babutskyi, et al. (17)). Therefore, the magnetic treatment of AISI 1045 steel accelerated oxidation of the worn surfaces and debris and changed the wear condition from severe to mild wear. In addition, the magnetic domain structure changed under normal load, with the balance of magnetostatic energy inside the material disrupted, which causes a micromagnetic field outside the material (Hase and Mishina (40)). The size and quantity of transfer particles formed on the worn surfaces during friction increased, resulting in greater magnetic flux density on the worn surfaces with increased normal load. The closed magnetic route of the ball–debris–disk body was generated because the ball was in close proximity to the wear debris. During the friction and wear processes, sheets of wear debris were rubbed repeatedly on the worn surfaces. With ongoing friction, the oxide film and wear debris prevented direct metal–metal contact when oxidation of the worn surfaces and refinement of wear debris reached a certain degree, which is the main cause of the transition from severe to mild wear (Han, et al. (18)). In mild wear, the friction torque was decreased due to the third-body lubricant formed by the minute and loose wear debris. As the wear test progressed, wear particles were extruded onto the worn surfaces to form a continuous, compressed, friction-reducing antiwear layer that possessed improved toughness and prevented direct metal–metal contact.

In boundary lubrication theory, the formation of an adsorption layer or generation of a surface chemical reaction film is the dominant factor in reducing friction and wear. EDS analysis of the tribofilm formed by additive-modified lubricants demonstrated that, under boundary lubrication conditions, some additives adsorbed onto the worn surfaces and others decomposed and reacted with the worn surfaces during friction to form a tribofilm, resulting in reduced friction and wear (Feng and Xia (37)). According to previous studies (Han, et al. (18); Jiang,
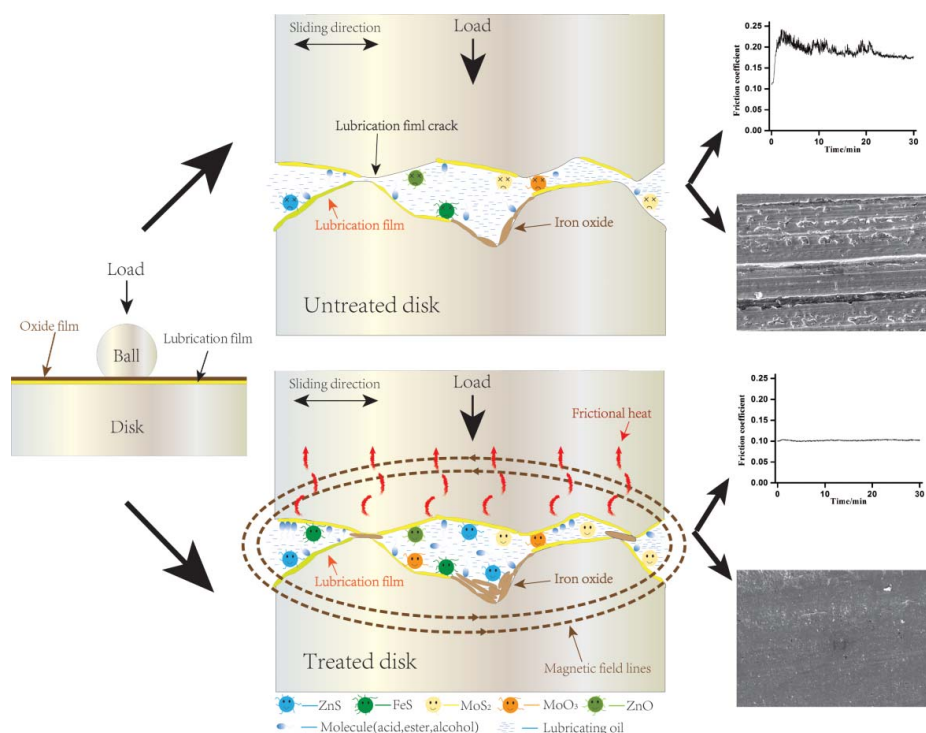

Figure 12. Schematic of dynamic friction mechanism of untreated and treated samples.

et al. (*19*); Abdeljaber, et al. (*41*)), magnetic fields could promote tribological chemical reactions, which were attributed to the following reasoning. Oxide particles were frequently crushed between surfaces and fresh metal was continuously exposed, such that, under these rigorous conditions, additives reacted more actively with freshly exposed metal surfaces to generate a more effective tribofilm. Then the tribofilm carrying capacity on the treated surface improved, such that the worn surfaces of treated disks were flat and their real-time friction coefficients were stable. By comparison, without the effects of micromagnetic fields, the worn surfaces of untreated disks were uneven and the real-time friction coefficients were unstable, which was attributed to cracking of the tribofilm under high normal load during sliding. In conclusion, both the adsorbed and chemical layers on the treated disk surfaces played antifriction and antiwear roles during the sliding process, leading to better lubrication effects.

There is also a relationship between the static mechanism and dynamic mechanism. Magnetization results in grain refinement and increased dislocation density. These microstructural changes increase the material's hardness and improve its antiwear property. The worn surface will be flat, which results in a stable and low friction coefficient. In this lubricating condition, the tribofilm is not easy to break up, especially when the normal load reaches 200 N.

Conclusion

1. The mechanism that alters mechanical and tribological properties of AISI 1045 steel by pulsed magnetic treatment was studied. A series of mechanical and tribological experiments was carried out before and after pulsed magnetic treatment of steel samples. AISI 1045 steel material exhibited improved mechanical properties after magnetic treatment, which produced increased microhardness. In addition, dislocation densities of treated samples were higher than those of untreated samples, and refined ferrite crystals were found in the microstructure, which resulted in improved mechanical properties.

2. With additive-modified lubricants, both the friction coefficients and wear widths of all samples clearly decreased relative to base oil lubrication alone. The tribological properties of treated samples were much better than those of untreated samples, which was attributed to the generation of a tribofilm. Micromagnetic fields on the worn surfaces served to activate the tribofilm generation process.

3. Micromagnetic fields attracted wear debris to the surface, which was then rubbed repeatedly and thinned constantly, promoting oxidation of wear debris. Then, a compacted oxide film formed to transform metal-to-metal contact into oxide film–to–oxide film contact. In addition, the wear mechanism was changed from severe abrasive and adhesive wear to mild abrasive and adhesive wear.

Acknowledgment

Funding

References

(1) Haftlang, F., Habibolahzadeh, A., and Sohi, M. H. (2015), "Improving Electrochemical Properties of AISI 1045 Steels by Duplex Surface Treatment of Plasma Nitriding and Aluminizing," *Applied Surface Science*, **329**, pp 240–247.

(2) Xia, Y. Q., Wang, L. P., Liu, X. Q., and Qiao, Y. L. (2008), "A Comparative Study on the Tribological Behavior of Nanocrystalline Nickel and Coarse-Grained Nickel Coatings under Ionic Liquid Lubrication," *Tribology Letters*, **30**(2), pp 151–157.

(3) Xia, Y. Q., Liu, W. M., Yu, L. G., Han, N., and Xue, Q. J. (2003), "Investigation on the Tribological Properties of Boron and Lanthanum Permeated Mild Steel," *Materials Science and Engineering A*, **354**(1), pp 17–23.

(4) Xia, Y. Q., Liu, W. M., and Xue, Q. J. (2005), "Comparative Study of the Tribological Properties of Various Modified Mild Steels under Boundary Lubrication Condition," *Tribology International*, **38**(5), pp 508–514.

(5) Jia, Z. F., Xia, Y. Q., Li, J. L., Pang, X. J., and Shao, X. (2010), "Friction and Wear Behavior of Diamond-Like Carbon Coating on Plasma Nitrided Mild Steel under Boundary Lubrication," *Tribology International*, **43**(1), pp 474–482.

(6) Jia, Z. F., Xia, Y. Q., Pang, X. J., and Hao, J. Y. (2011), "Tribological Behaviors of Different Diamond-Like Carbon Coatings on Nitrided Mild Steel Lubricated with Benzotriazole-Containing Borate Esters," *Tribology Letters*, **41**(1), pp 247–256.

(7) Jia, Z. F., Wang, L. P., Xia, Y. Q., Zhang, H. B., Pang, X. J., and Li, B. (2009), "Tribological Behaviors of Diamond-Like Carbon Coatings on Plasma Nitrided Steel Using Three BN-Containing Lubricants," *Applied Surface Science*, **255**(13), pp 6666–6674.

(8) Ma, L. P., Liang, Z. Q, Wang, X. B., Zhao, W. X., Zhou, T. F., and Yao, H. M. (2013), "Effect of Low-Frequency Pulsed Magnetic Treatment on Micro-Hardness of High Speed Steel," *Advanced Materials Research*, **797**, pp 663–666.

(9) Ma, L. P., Zhao, W. X., Liang, Z. Q., Wang, X. B., Xie, L. J., Jiao, L., and Zhou, T. F. (2014), "An Investigation on the Mechanical Property Changing Mechanism of High Speed Steel by Pulsed Magnetic Treatment," *Materials Science and Engineering A*, **609**, pp 16–25.

(10) Liang, Z. Q., Ma, L. P., Wang, X. B., Zhao, W. X., Zhou, T. F., Yan, P., and Jiao, L. (2015), "Influence of Pulsed Magnetic Treatment on Wear of Carbide Micro-End-Mill," *Advanced Materials Research*, **806**, pp 143–148.

(11) Nabi, B., Helbert, A. L., Brisset, F., Andre, G., Waeckerle, T., and Baudin, T. (2013), "Effect of Recrystallization and Degree of Order on the Magnetic and Mechanical Properties of Soft Magnetic FeCo-2V Alloy," *Materials Science and Engineering A*, **578**(9), pp 215–221.

(12) Mikhalitsyna, E. A., Kataev, V. A., Larrañaga, A., Lepalovskij, V. N., and Turygin, A. P. (2016), "Microstructure and Magnetic Properties of $Fe_{72.5}Si_{14.2}B_{8.7}Nb_2Mo_{1.5}Cu_{1.1}$ Thin Films," *Journal of Magnetism and Magnetic Materials*, **415**, pp 61–65.

(13) Cai, Z. and Huang, X. (2011), "Residual Stress Reduction by Combined Treatment of Pulsed Magnetic Field and Pulsed Current," *Materials Science and Engineering A*, **528**(19–20), pp 6287–6292.

(14) Liang, Z. Q., Ma, L. P., Wang, X. B., Xie, L. J., Zhao, W. X., and Yao, H. M. (2015), "The Effect of Pulsed Magnetic Field on Friction and Wear Properties of High Speed Steel Tool Materials," *Acta Armamentarii*, **36**(5), pp 904–910.

(15) Wei, Y., Zhang, Y., Chen, Y., and Du, S. (2013), "Impact of Material Permeability on Friction and Wear Properties under the Interference of DC Steady Magnetic Field," *Tribology International*, **57**(4), pp 162–169.

(16) Tharajak, J. and Nicomrat, D. (2016), "Friction Coefficient and Worn Surface of Ferromagnetic Materials under Magnetic Fields," *Applied Mechanics and Materials*, **848**, pp 31–34.

(17) Babutskyi, A., Chrysanthou, A., and Zhao, C. (2014), "Effect of Pulsed Magnetic Field Pre-Treatment of AISI 52100 Steel on the

Coefficient of Sliding Friction and Wear in Pin-on-Disk Tests," *Friction*, **2**(4), pp 310–316.

(18) Han, H., Gao, Y., Zhang, Y., Du, S., and Liu, H. (2015), "Effect of Magnetic Field Distribution of Friction Surface on Friction and Wear Properties of AISI 1045 Steel in DC Magnetic Field," *Wear*, 328–329, pp 422–435.

(19) Jiang, J., Tian, Y., and Meng, Y. (2011), "Role of External Magnetic Field during Friction of Ferromagnetic Materials," *Wear*, **271**(11–12), pp 2991–2997.

(20) Du, S., Yue, W., Wang, Y., She, D., Huang, H., and Fu, Z. (2015), "Synergistic Effects between Sulfurized–Nanocrystallized 316L Steel and MoDTC Lubricating Oil Additive for Improvement of Tribological Performances," *Tribology International*, **94**, pp 530–540.

(21) Wang, Y., Yue, W., She, D., Fu, Z., Huang, H., and Liu, J. (2014), "Effects of Surface Nanocrystallization on Tribological Properties of 316L Stainless Steel under MoDTC/ZDDP Lubrications," *Tribology International*, **79**(11), pp 42–51.

(22) Parsaeian, P., Ghanbarzadeh, A., Wilson, M., Eijk, M. C. P. V., Nedelcu, I., Dowson, D., Neville, A., and Morina, A. (2016), "An Experimental and Analytical Study of the Effect of Water and Its Tribochemistry on the Tribocorrosive Wear of Boundary Lubricated Systems with ZDDP-Containing Oil," *Wear*, 358–359, pp 23–31.

(23) Miyake, K., Kume, T., Nakano, M., Korenaga, A., Takiwatari, K., Tsuboi, R., and Sasaki, S. (2012), "Effects of Surface Chemical Properties on the Frictional Properties of Self-Assembled Monolayers Lubricated with Oleic Acid," *Tribology Online*, **7**(4), pp 214–224.

(24) Xu, X. C., Xia, Y. Q., Wu, H., and Chen, G. X. (2014), "The Tribological Properties of Plant Leaf Extracts as Lubricant Additives for an Aluminum-on-Steel Contact," *Chinese Science Bulletin*, **36**, pp 3624–3625.

(25) Xia, Y. Q., Xu, X. C., Feng, X., and Chen, G. X. (2015), "Leaf-Surface Wax of Desert Plants as a Potential Lubricant Additive," *Friction*, **3**(3), pp 208–213.

(26) Williamson, G. K. and Smallman, R. E. (1956), "Dislocation Densities in Some Annealed and Cold-Worked Metals from Measurements on the X-ray Debye-Scherrer Spectrum," *Philosophical Magazine*, **1**(1), pp 34–36.

(27) Hahn, J. D., Wu, F., and Bellon, P. (2004), "Cr-Mo Solid Solutions Forced by High-Energy Ball Milling," *Metallurgical and Materials Transactions A*, **35**(13), pp 1105–1111.

(28) Biju, V., Sugathan, N., Vrinda, V., and Salini, S. L. (2008), "Estimation of Lattice Strain in Nanocrystalline Silver from X-ray Diffraction Line Broadening," *Journal of Materials Science*, **43**(4), pp 1175–1179.

(29) Tan, X., Xu, Y., Yang, X., and Wu, D. (2014), "Microstructure–Properties Relationship in a One-Step Quenched and Partitioned Steel," *Materials Science and Engineering A*, **589**(2), pp 101–111.

(30) Wang, Z. and Wang, Y. (2011), "Existence of Quasiperiodic Solutions and Littlewood's Boundedness Problem of Super-Linear Impact Oscillators," *Applied Mathematics and Computation*, **217**(13), pp 6417–6425.

(31) Klamecki, B. E. (2003), "Residual Stress Reduction by Pulsed Magnetic Treatment," *Journal of Materials Processing Technology*, **141**(3), pp 385–394.

(32) Ma, L. P., Liang, Z. Q., Wang, X. B., Zhao, W. X., Jiao, L., and Liu, Z. B. (2015), "Influence of Pulsed Magnetic Treatment on Microstructures and Mechanical Properties of M42 High Speed Steel Tool," *Acta Metallurgica Sinica*, **63**(1), pp 137–145.

(33) Stolarski, T. A. and Makida, Y. (2011), "Influence of Permanent Magnetic Field on Wear Performance of Dry Sliding Contacts," *Wear*, **271**(7–8), pp 1109–1123.

(34) Kano, M., Martin, J. M., Yoshida, K., and Bouchet, M. I. D. B. (2014), "Super-Low Friction of ta-C Coating in Presence of Oleic Acid," *Friction*, **2**(2), pp 156–163.

(35) Okubo, H., Tadokoro, C., and Sasaki, S. (2015), "Tribological Properties of a Tetrahedral Amorphous Carbon (ta-C) Film under Boundary Lubrication in the Presence of Organic Friction Modifiers and Zinc Dialkyldithiophosphate (ZDDP)," *Wear*, 332–333, pp 1293–1302.

(36) Wang, J., Chen, B., Yan, F., Xue, Q., and Zhao, F. (2011), "Pattern Abrasion of Ultra-High Molecular Weight Polyethylene: Microstructure Reconstruction of Worn Surface," *Wear*, **272**(1), pp 176–183.

(37) Feng, X. and Xia, Y.Q. (2012), "Tribological Properties of Non-Ferrous Coating Lubricated with Rapeseed Oil Containing Lubricant Additives," *Lubrication Science*, **24**(8), pp 361–371.

(38) Yang, Y., Zhang, C., Wang, Y., Dai, Y., and Luo, J. (2016), "Friction and Wear Performance of Titanium Alloy against Tungsten Carbide Lubricated with Phosphate Ester," *Tribology International*, **95**, pp 27–34.

(39) Filho, I. R. S., Sandim, M. J. R., Cohen, R., Nagamine, L. C. C. M., Hoffmann, J., Bolmaro, R. E., and Sandim, H. R. Z. (2016), "Effects of Strain-Induced Martensite and Its Reversion on the Magnetic Properties of AISI 201 Austenitic Stainless Steel," *Journal of Magnetism and Magnetic Materials*, **419**, pp 156–165.

(40) Hase, A. and Mishina, H. (2010), "Magnetization of Friction Surfaces and Wear Particles under Tribological Processes," *Wear*, **268**(1–2), pp 370–371.

(41) Abdeljaber, G. T., Mohamed, M. K., and Ali, W. Y. (2014), "Effect of Magnetic Field on the Friction and Wear of Polyamide Sliding against Steel," *Materials Sciences and Applications*, **5**(1), pp 46–53.